A novel approach to modelling and simulating the contact behaviour between a human hand model and a deformable object

Dominique Chamoret, Sébastien Roth, Zhi-Qiang Feng, Xiu-Tian Yan, Samuel Gomes,, François Peyraut

A novel approach to modelling and simulating the contact behaviour between a human hand model and a deformable object

D. Chamoret[a]*, S. Roth[a], Z.-Q. Feng[b,c], X.-T. Yan[d], S. Gomes[a] and F. Peyraut[a]

[a]Laboratoire M3M, Université de Technologie de Belfort-Montbéliard, 90010 Belfort, France; [b]School of Mechanics and Engineering, Southwest Jiaotong University, Chengdu, China; [c]Laboratoire LMEE, Université d'Evry, 91020 Evry, France; [d]Department of Design, Manufacture and Engineering Management, James Weir Building, University of Strathclyde, 75 Montrose Street, Glasgow, UK

A deeper understanding of biomechanical behaviour of human hands becomes fundamental for any human hand-operated activities. The integration of biomechanical knowledge of human hands into product design process starts to play an increasingly important role in developing an ergonomic product-to-user interface for products and systems requiring high level of comfortable and responsive interactions. Generation of such precise and dynamic models can provide scientific evaluation tools to support product and system development through simulation. This type of support is urgently required in many applications such as hand skill training for surgical operations, ergonomic study of a product or system developed and so forth. The aim of this work is to study the contact behaviour between the operators' hand and a hand-held tool or other similar contacts, by developing a novel and precise nonlinear 3D finite element model of the hand and by investigating the contact behaviour through simulation. The contact behaviour is externalised by solving the problem using the bi-potential method. The human body's biomechanical characteristics, such as hand deformity and structural behaviour, have been fully modelled by implementing anisotropic hyperelastic laws. A case study is given to illustrate the effectiveness of the approach.

Keywords: contact; impact; anisotropic hyperelasticity; biomechanics; finite element analysis

1. Introduction

In today's well-developed professional operations and competitive market place, it is vital to put stakeholders at the heart of the design of a new product, system or process in order to develop most suitable man–machine interfaces (MMI). This is especially the case when skilful hand manipulation is required to handle delicate objects of interests. One such an example is the medical surgical operations on a patient (Misra et al. 2010), where a surgeon needs to utilise and interact with medical instruments with good MMI in order to perform the highest possible quality operations for patients. In these applications, it is appropriate and desirable to model human hands in order to gain a deeper understanding of the hand operations. To model such a hand, it is appropriate to deploy proven methods and tools such as finite element (FE) method to integrate biomechanical knowledge into the existing design process to produce an efficient solution with better MMI. The aim of our work is to study the contact pressure between the hand and an object when operators handle the object using hand-held tools or planning and training aids, such as a haptic device, by developing a nonlinear 3D FE model of the hand and to derive optimised procedures for analyses. The precise pressure map of the contacts and the dynamic change of these pressures are the critical focal points of the study as an accurate computer-simulated representation would provide a powerful tool to study contacts for many ergonomic-centred studies for product, system and process development. In these applications, it is very important and interesting to evaluate the magnitudes and to determine the locations of these high pressures (Thalmann and Thalmann 1995), which require realistic modelling of the deformation of soft tissues. This problem can be very complex and challenging because of the presence of two principles of strongly nonlinear phenomena: contact and hyperelasticity.

Problems involving unilateral contact and friction are among the most difficult ones in mechanics. The treatment of contact conditions leads to variational inequalities. A large number of algorithms to solve these problems by the FE method have been presented in the literature (Alart and Curnier 1991; Simo and Laursen 1992). In this paper, the so-called bi-potential method is used as the basis of the approach. The novel aspect of our approach is the extension of the above approach to dynamic contact problems by using an appropriate time integration algorithm (Feng et al. 2006, 2007).

This paper is structured as follows. In Section 2, the solution method of contact problems is outlined. The FE formulation of large hyperelastic deformation including anisotropic effects is presented in Section 3. In Section 4,

*Corresponding author. Email: dominique.chamoret@utbm.fr

different steps of how to generate a 3D hand model from medical image are explained. This model is then used to interact with a deformable object and the results are shown in Section 5. Finally, some conclusions are drawn from this study.

2. Methods

2.1 Contact modelling

2.1.1 Definition

Let us consider two deformable bodies in potential contact, and the two potential contact surfaces are noted Γ and Γ'. Let $\mathbf{x} = \varphi(\mathbf{X}, t)$ be the current position vector at an instant $t \in \mathbf{I}_t$. The orthogonal projection of $\mathbf{x}$ on the body surface Γ' is defined by $\mathbf{x}'$. The contact distance vector (or gap vector) is defined by

$$\mathbf{g} = \mathbf{x} - \mathbf{x}' = h\mathbf{n}, \tag{1}$$

where h is the oriented contact distance (Figure 1). The displacement vector $\mathbf{u}$, the velocity vector $\dot{\mathbf{u}}$ and the contact stress vector $\mathbf{r}$ can be uniquely decomposed into a normal part and a tangential part as follows (Figure 1):

$$\mathbf{u} = \mathbf{u}_t + u_n\mathbf{n}, \quad u_n = \mathbf{u}\cdot\mathbf{n}, \tag{2}$$

$$\dot{\mathbf{u}} = \dot{\mathbf{u}}_t + \dot{u}_n\mathbf{n}, \quad \dot{u}_n = \dot{\mathbf{u}}\cdot\mathbf{n}, \tag{3}$$

$$\mathbf{r} = \mathbf{r}_t + r_n\mathbf{n}, \quad r_n = \mathbf{r}\cdot\mathbf{n}. \tag{4}$$

The unilateral contact law is characterised by a geometric condition of non-penetration, a static condition of no-adhesion and a mechanical complementary condition. These three conditions, known as the Signorini conditions, can be formulated as

$$h \geq 0, \quad r_n \geq 0, \quad hr_n = 0. \tag{5}$$

In general, at any time $t \in \mathbf{I}_t$, the potential contact surfaces Γ can be split into two disjoint parts: ${}^{+}\Gamma$, where the body is in contact with Γ', and ${}^{-}\Gamma$, where the body is separated from Γ'. In the case of dynamic contact, the Signorini conditions can be formulated, on ${}^{+}\Gamma$, via the relative velocity

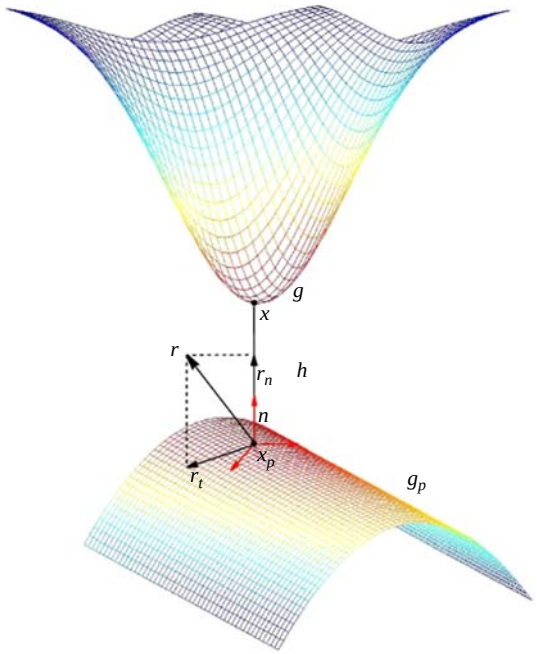

Figure 1. Description of contact problem.

$$\dot{u}_n \geq 0, \quad r_n \geq 0, \quad \dot{u}_n r_n = 0 \text{ on } {}^{+}\Gamma. \tag{6}$$

The bodies are separated when $\dot{u}_n > 0$ and remain in contact for $\dot{u}_n = 0$.

Formulation (6) of the Signorini conditions can be combined with the sliding rule to derive the complete frictional contact law for the contacting part ${}^{+}\Gamma$. This complete law specifies possible velocities of bodies that satisfy the unilateral contact conditions and the sliding rule. In this work, the classical isotropic Coulomb friction rule is used. The set of admissible forces, denoted by Coulomb's convex cone K_μ, is defined by

$$K_\mu = \left\{\mathbf{r} \in \mathcal{R}^3 \text{ such that } |\mathbf{r}_t| - \mu r_n \leq 0\right\}. \tag{7}$$

On the contacting surface ${}^{+}\Gamma$, the sliding rule can be combined with the Signorini conditions to obtain the frictional contact law that specifies possible scenarios on the contact area (stick, slip and separation). Two overlapped 'if…then…else' statements can be used to write it in a compact form:

$$\begin{array}{lll}
\text{if} & r_n = 0 \text{ then } \dot{u}_n \geq 0 & \text{! separating} \\
\text{else if} & \mathbf{r} \in \operatorname{int} K_\mu \text{ then } \dot{u}_n = 0 \text{ and } -\dot{\mathbf{u}}_t = \mathbf{0}, & \text{! sticking} \\
\text{else} & (\mathbf{r} \in \operatorname{bd} K_\mu \text{ and } r_n > 0) & \\
 & \left\{\dot{u}_n = 0 \text{ and } \exists\dot{\lambda} > 0 \text{ such that } -\dot{\mathbf{u}}_t = \dot{\lambda}\frac{\mathbf{r}_t}{|\mathbf{r}_t|}\right\}, & \text{! sliding} \\
\text{end if} & &
\end{array} \quad , \tag{8}$$

where '$\operatorname{int} K_\mu$' and '$\operatorname{bd} K_\mu$' denote the interior and the boundary of K_μ, respectively.

It is noted that the minus sign before $\dot{\mathbf{u}}_t$ means that the frictional force is opposite to the sliding velocity in the isotropic friction case. The complete form of the frictional contact law involves three possible states, which are separating, contact with sticking and contact with sliding. Only the last state produces energy dissipation.

2.1.2 Numerical solution

The numerical treatment of the contact constraints is based on two main strategies: the penalty method and the regularisation method (the Lagrange multipliers). Both approaches have their advantages and their drawbacks. These methods can be easily implemented in an existing FE code, but the choice of good parameters is often difficult (Chamoret et al. 2004).

In this paper, we have chosen to use an original approach, the bi-potential method.

De Saxcé and Feng (1998) have shown that the contact law (8) is equivalent to the following differential inclusion:

$$\begin{aligned} &\left(-\dot{\mathbf{u}}_t - (\dot{u}_n + \mu|-\dot{\mathbf{u}}_t|)\mathbf{n}\right) \in \partial \bigcup_{K_\mu} \mathbf{r}, \\ &\text{where } \bigcup_{K_\mu}(\mathbf{r}) = \begin{cases} 0, & \text{if } \mathbf{r} \in K_\mu \\ +\infty & \text{otherwise.} \end{cases} \end{aligned} \tag{9}$$

Then, the following contact bi-potential can be defined:

$$b_c(-\dot{\mathbf{u}}, \mathbf{r}) = \bigcup_{\mathbb{R}_-}(-\dot{u}_n) + \bigcup_{K_\mu}(\mathbf{r}) + \mu r_n|-\dot{\mathbf{u}}_t|. \tag{10}$$

In order to avoid non-differentiable potentials that occur in nonlinear mechanics, such as in contact problems, it is convenient to use the augmented Lagrangian method (Alart and Curnier 1991; Simo and Laursen 1992). For the contact bi-potential b_c, given by (10), the modified augmented surface traction $\boldsymbol{\tau}$ is defined by

$$\boldsymbol{\tau} = \mathbf{r} + \varrho\left(-\dot{\mathbf{u}}_t - (\dot{u}_n + \mu|-\dot{\mathbf{u}}_t|)\mathbf{n}\right), \tag{11}$$

where $\varrho > 0$ is a numerical parameter that is determined to ensure numerical convergence. It can be shown that $\mathbf{r}$ is the projection of $\boldsymbol{\tau}$ onto the closed convex Coulomb's cone:

$$\mathbf{r} = \operatorname{proj}(\boldsymbol{\tau}, K_\mu). \tag{12}$$

For the numerical solution of the implicit Equation (12), the Uzawa or Newton algorithm can be used (Joli and Feng 2008).

2.2 Anisotropic hyperelastic constitutive law

2.2.1 Anisotropic hyperelasticity

To investigate the internal deformation and the stress of biological soft tissues, such as ligaments, tendons or arterial walls, anisotropic hyperelastic constitutive laws are often used in the framework of an FE analysis (Weiss et al. 1996; Almeida and Spilker 1998; Rüter and Stein 2000). The most used strain energy functions take a power law form (Schröder et al. 2005) or present an exponential behaviour (Fung et al. 1979; Holzapfel et al. 2000). More recently, Balzani et al. (2006) have proposed polyconvex strain energy functions combining an exponential form with a power law to take care of the tissues behaviour in the low load domain. More realistic models have also been recently developed to capture the inter-fibre angle change in addition to the contribution of the fiber–matrix shear interaction of the strain energy (Peng et al. 2006). In general, the anisotropy can be represented via the introduction of a so-called structural tensor, which allows a coordinate-invariant formulation on the constitutive equations (Boehler 1987; Spencer 1987; Zheng and Spencer 1993). It is usually assumed that anisotropy is due to collagen fibres behaviour (Gasser et al. 2006), while the ground substance, or matrix, behaves in an isotropic manner, so the energy densities modelling transversely isotropic and orthotropic soft tissues are separated into isotropic and anisotropic parts (Weiss et al. 1996; Balzani et al. 2006)

$$W = W_{\text{iso}} + \sum_{a=1}^{n} W^a_{\text{ani}}. \tag{13}$$

Each anisotropic density W^a_{ani} refers to a preferred direction of the material. The number of fibre families n is generally set to 1 to model tissues as ligaments or tendons, whereas it is set to 2 to represent the behaviour of arterial walls.

In continuation, $\mathbf{C} = \mathbf{F}^T\mathbf{F}$ is the right Cauchy–Green deformation tensor and $\mathbf{F}$ is the transformation gradient defined by

$$\mathbf{F} = \frac{\partial \mathbf{x}}{\partial \mathbf{X}} = \mathbf{I} + \frac{\partial \mathbf{u}}{\partial \mathbf{X}}, \quad J = \det(\mathbf{F}) > 0, \tag{14}$$

where $\mathbf{X}$, $\mathbf{x}$ and $\mathbf{u}$ represent the reference position, the current position and the displacement vector of a material point, respectively.

According to Zhang–Rychlewski's theorem (Zhang and Rychlewski 1990), the condition of material symmetry is satisfied if structural tensors are additionally included in the strain energy density representation. Transversely, isotropic densities can then be expressed with the three invariants I_1, I_2 and I_3 of the right Cauchy–Green deformation tensor $\mathbf{C}$ and the two additional mixed invariants J_4 and J_5 (Boehler 1987; Spencer 1987; Zheng

and Spencer 1993)

$$I_1 = \mathrm{tr}\,(\mathbf{C}), \quad I_2 = \mathrm{tr}\,(\mathrm{cof}(\mathbf{C})), \quad I_3 = \det(\mathbf{C})$$
$$J_4 = \mathrm{tr}\,(\mathbf{CM}), \qquad J_5 = \mathrm{tr}\,(\mathbf{C}^2\mathbf{M}), \tag{15}$$

where $\mathrm{cof}(\mathbf{C})$ denotes the cofactor matrix of $\mathbf{C}$ and $\mathbf{M}$ is the so-called structural tensor representing the transverse-isotropy group and referring to a preferred direction $\mathbf{a}$ of the material

$$\mathbf{M} = \mathbf{a} \otimes \mathbf{a}. \tag{16}$$

It is noted that (15) and (16) give

$$J_4 = \mathrm{tr}\left(\mathbf{F}^T\mathbf{F}\,\mathbf{a} \otimes \mathbf{a}\right) = \|\mathbf{Fa}\|^2. \tag{17}$$

The double brackets represent the usual Euclidian norm. The square root of J_4 represents thus the stretch in the fibre direction.

In the case of hyperelastic materials, there exists an elastic potential function W, which is a scalar function of the strain tensors. The second Piola–Kirchhoff stress tensor $\mathbf{S}$ and the corresponding Cauchy stress tensor $\boldsymbol{\sigma}$ are given by

$$\mathbf{S} = \frac{\partial W}{\partial \mathbf{E}} = 2\frac{\partial W}{\partial \mathbf{C}}, \quad \boldsymbol{\sigma} = \frac{1}{J}\mathbf{F}\mathbf{S}\mathbf{F}^T. \tag{18}$$

In this relation, $\mathbf{E}$ is the Green–Lagrangian strain tensor that given by the classical relation:

$$\mathbf{E} = \frac{1}{2}(\mathbf{C} - \mathbf{I}), \tag{19}$$

where $\mathbf{I}$ is the second-order unit tensor.

To uncouple the deviatoric part to the dilatational part of the response, the volume preserving part $\bar{\mathbf{F}} = J^{-1/3}\mathbf{F}$ of the deformation is introduced (Weiss et al. 1996). The modified invariants related to $\bar{\mathbf{C}} = \bar{\mathbf{F}}^T\bar{\mathbf{F}} = J^{-2/3}\mathbf{C}$ are expressed from (15) by

$$\bar{I}_1 = I_1 I_3^{-1/3}, \quad \bar{I}_2 = I_2 I_3^{-2/3},$$
$$\bar{J}_4^a = J_4^a I_3^{-1/3}, \quad \bar{J}_5^a = J_5^a I_3^{-2/3}. \tag{20}$$

The exponential type HGO density adopted in this work uses these modified invariants as follows:

$$W = \bar{W}(\bar{I}_1, \bar{J}_4^a) + U(J), \tag{21}$$

$$U(J) = \frac{k}{2}(J-1)^2; \bar{W}(\bar{I}_1, \bar{J}_4^a) = W_{\mathrm{iso}}(\bar{I}_1) + \sum_{a=1}^{2} W_{\mathrm{ani}}(\bar{J}_4^a); W_{\mathrm{iso}}(\bar{I}_1) = c_1(\bar{I}_1 - 3), \tag{22}$$

$$J_4^a < 1 : W_{\mathrm{ani}}(\bar{J}_4^a) = 0, \tag{23}$$

$$J_4^a \geq 1 : W_{\mathrm{ani}}(\bar{J}_4^a) = \frac{k_1}{2k_2}\left[\exp\left(k_2(\bar{J}_4^a - 1)^2\right) - 1\right]. \tag{24}$$

The anisotropic energy density W_{ani} is case sensitive with respect to J_4 because the case $J_4 < 1$ represents the shortening of the fibres, which is assumed to generate no stress. The proof of convexity of (23) and (24) with respect to $\mathbf{F}$ is given by Schröder et al. (2005) and Peng et al. (2006). The non-collagenous matrix of the media is modelled by the neo-Hookean isotropic density W_{iso} defined by (22). It is noted that the volumetric–isochoric split of the above HGO model does only hold for (quasi) incompressible deformations. An extension to compressible deformations would require that the volumetric part of the strain energy function includes a dependency on the structural tensor. This is proved recently by Guo et al. (2008), where a simple compressible anisotropic analytical model is developed. The parameter values c_1, k_1 and k_2 of the material have been chosen as similar to those mentioned in Balzani et al. (2006) in order to fit the model with experimental data: $c_1 = 10.2069$, $k_1 = 0.0017$ and $k_2 = 882.847\,\mathrm{kPa}$. These parameters are assumed to be independent of the fibre orientation. This hypothesis is consistent since the fibre properties are assumed to be independent of their orientation.

The dilatational component $U(J)$ defined by Equation (22) represents a penalty term added to the FE model to account for the incompressible behaviour of the material. The parameter k was chosen equal to 10^5. We remind finally that by deriving W from Equation (18) and introducing the matrix of cofactors of $\mathbf{C}$, $\mathrm{cof}(\mathbf{C}) = I_3\mathbf{C}^{-T}$, it is conventionally obtained

$$\mathbf{S} = 2\left[\frac{\partial W}{\partial I_1}\mathbf{I} + \frac{\partial W}{\partial I_2}(I_1\mathbf{I} - \mathbf{C}) + \frac{\partial W}{\partial I_3}\mathrm{cof}(\mathbf{C}) + \frac{\partial W}{\partial J_4^1}\mathbf{M}^{\mathbf{a}^1} + \frac{\partial W}{\partial J_4^2}\mathbf{M}^{\mathbf{a}^2} + \frac{\partial W}{\partial J_5^1}\left(\mathbf{C}\mathbf{M}^{\mathbf{a}^1} + \mathbf{M}^{\mathbf{a}^1}\mathbf{C}\right) + \frac{\partial W}{\partial J_5^2}\left(\mathbf{C}\mathbf{M}^{\mathbf{a}^2} + \mathbf{C}\mathbf{M}^{\mathbf{a}^2}\right)\right]. \tag{25}$$

In our particular case, Equation (25) is reduced to

$$\mathbf{S} = 2\left[\frac{\partial W}{\partial \mathrm{I}_1}\mathbf{I} + \frac{\partial W}{\partial I_3}\mathrm{cof}(\mathbf{C}) + \frac{\partial W}{\partial J_4^1}\mathbf{M}^{\mathbf{a}^1} + \frac{\partial W}{\partial J_4^2}\mathbf{M}^{\mathbf{a}^2}\right]. \tag{26}$$

The derivatives of the density energy W with respect to the invariants are described by Peyraut et al. (2010). The stress tensor (26) and the first derivatives of the energy density with respect to the invariants will be used to evaluate the tangent modulus. These moduli are useful to implement hyperelastic models in an FE code. The implementation of the HGO model in the in-house FE code FER is presented in Section 2.2.2.

2.2.2 FE implementation of the HGO model

The HGO model has been implemented and tested in the FE code FER/Impact. This code is implemented

using C++ object-oriented programming language. In the context of large hyperelastic displacement and rotations, the Green–Lagrangian strain tensor is used to describe the nonlinear strain–displacement relationship:

$$\mathbf{E} = \left(\mathbf{B}_{\mathrm{L}} + \frac{1}{2}\mathbf{B}_{\mathrm{NL}}(\mathbf{u})\right)\mathbf{u}, \tag{27}$$

where $\mathbf{B}_L$ is the matrix that relates the linear strain term to the nodal displacements and $\mathbf{B}_{\mathrm{NL}}(\mathbf{u})$ is the matrix that relates the nonlinear strain term to the nodal displacements. The incremental form of the strain–displacement relationship is

$$\delta\mathbf{E} = (\mathbf{B}_{\mathrm{L}} + \mathbf{B}_{\mathrm{NL}}(\mathbf{u}))\delta\mathbf{u}. \tag{28}$$

Using Equations (18) and (28), the incremental form of the stress $\delta\mathbf{S}$ can be linked to the incremental form of the strain $\delta\mathbf{E}$ as follows:

$$\delta\mathbf{S} = \frac{\partial^2 W}{\partial \mathbf{E}^2} : \delta\mathbf{E} = \mathbf{D} : \delta\mathbf{E} = \mathbf{D} : (\mathbf{B}_{\mathrm{L}} + \mathbf{B}_{\mathrm{NL}}(\mathbf{u}))\delta\mathbf{u}, \tag{29}$$

where $\mathbf{D}$ denotes the constitutive tangent matrix. This fourth-order tensor is obtained from the derivative of W (Schröder et al. 2005). Using the principle of virtual displacement, the virtual work δU is given as

$$\begin{aligned}\delta U = {} & \delta\mathbf{u}^{\mathrm{T}}\mathbf{M}\ddot{\mathbf{u}} + \delta\mathbf{u}^{\mathrm{T}}\mathbf{A}\dot{\mathbf{u}} \\ & + \int_{V_0} \delta\mathbf{E}^{\mathrm{T}}\mathbf{S}\,\mathrm{d}V - \delta\mathbf{u}^{\mathrm{T}}\mathbf{F}_{\mathrm{ext}} - \delta\mathbf{u}^{\mathrm{T}}\mathbf{R} = 0,\end{aligned} \tag{30}$$

where V_0 is the volume of the initial configuration, $\mathbf{F}_{\mathrm{ext}}$ is the vector of external loads, $\mathbf{R}$ is the contact reaction vector, $\mathbf{M}$ is the mass matrix, $\mathbf{A}$ is the damping matrix, $\dot{\mathbf{u}}$ is the velocity vector and $\ddot{\mathbf{u}}$ is the acceleration vector.

The damping implemented in the FE code FER is a Rayleigh damping; it means the damping matrix $\mathbf{A}$ is a linear combination of the stiffness and mass matrix. Substituting (28) into Equation (30), we obtain

$$\begin{aligned}\delta W = {} & \delta\mathbf{u}^{\mathrm{T}}\Bigg(\mathbf{M}\ddot{\mathbf{u}} + \mathbf{A}\dot{\mathbf{u}} \\ & + \int_{V_0} (\mathbf{B}_{\mathrm{L}} + \mathbf{B}_{\mathrm{NL}}(\mathbf{u}))^{\mathrm{T}}\mathbf{S}\,\mathrm{d}V_0 - \mathbf{F}_{\mathrm{ext}} - \mathbf{R}\Bigg) = 0.\end{aligned} \tag{31}$$

The vector of internal forces is defined by

$$\mathbf{F}_{\mathrm{int}} = \int_{V_0} (\mathbf{B}_{\mathrm{L}} + \mathbf{B}_{\mathrm{NL}}(\mathbf{u}))^{\mathrm{T}}\mathbf{S}\,\mathrm{d}V. \tag{32}$$

Since $\delta\mathbf{u}$ is arbitrary, it can be deduced from (31),

$$\mathbf{M}\ddot{\mathbf{u}} + \mathbf{A}\dot{\mathbf{u}} + \mathbf{F}_{\mathrm{int}} - \mathbf{F}_{\mathrm{ext}} - \mathbf{R} = 0. \tag{33}$$

The initial conditions associated with the dynamic Equation (33) are

$$\dot{\mathbf{u}} = \dot{\mathbf{u}}_0 \quad \text{and} \quad \mathbf{u} = \mathbf{u}_0. \tag{34}$$

Dynamic Equation (33) can be integrated between time t and $t + \Delta t$ by using an explicit algorithm:

$$\mathbf{u}^{t+\Delta t} = \Delta t^2\mathbf{M}^{-1}\left(\mathbf{F}^t_{\mathrm{ext}} - \mathbf{F}^t_{\mathrm{int}} + \mathbf{R}^{t+\Delta t}\right) + 2\mathbf{u}^t - \mathbf{u}^{t-\Delta t}. \tag{35}$$

It is possible to use special FE $Q1P0$ (Scovazzi et al. 2008) to achieve the element integration by separating the contributions from spherical and deviatoric stress. However, in the current version of FER, the integration of internal forces is the same as for the spherical and deviatoric parts, using 27 Gauss points for hexahedral elements and only 1 Gauss point for tetrahedral elements.

It should be noted that the contact reactions $\mathbf{R}$ are evaluated with the bi-potential method presented in Section 2.1. All the approaches presented in Sections 2.1 and 2.2 have been implemented in the FE code FER.

3. FE model

3.1 Creation of the hand model

The geometrical creation of the hand model is an integral part of the FE modelling. This geometrical representation is based on the geometric 3D reconstruction of slices of a hand obtained by a CT scanner. A tomodensitometry examination of the hand was performed on an adult subject for medical purposes with no relation with this study. No abnormalities were found by the medical staff. The acquisition of the 3D geometry was performed without injection with 2D reconstructions. Resolution of 2D slices was 0.7 mm. For the reconstruction, almost 300 slices in transversal plane were used. Figure 2 illustrates one CT slice of the hand. In order to distinguish the bones from the soft tissues, the slices processing was performed by using a grey-level processing, using the Scan2Mesh, which is a tool allowing 3D reconstruction, included in the HyperWorks package (Altair©).

In specifying the space between slices, the size of the pixels in each direction and the precision of the mesh, a 3D triangular mesh was generated and imported in HyperMesh v9.0 software (Altair©) for a step of surface reconstructions as illustrated in Figure 3 and for a step of 3D meshing as illustrated in Figure 4.

The hand includes wrist's and fingers' bones and the skin. In order to have a continuous meshing between every components, solids containing bones and skin have been created, and Boolean operations have been used, as presented in Figure 5.

Figure 2. CT slice of the hand.

Then an automatic mesh of the three components is performed by allowing a continuous mesh (without interfaces) between wrist's and fingers' bones and the skin.

Finally, the global mesh of the hand has 17,700 four-node tetra elements: 1700 elements in wrist's bones, 2000 elements in fingers' bones and 14,000 elements for the skin.

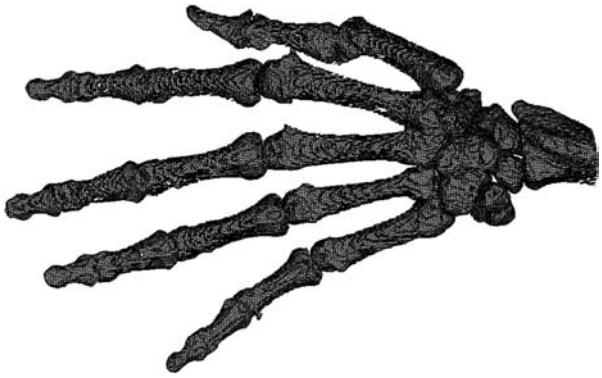

Figure 3. STL meshing of the hand with tria before the reconstruction of the surfaces.

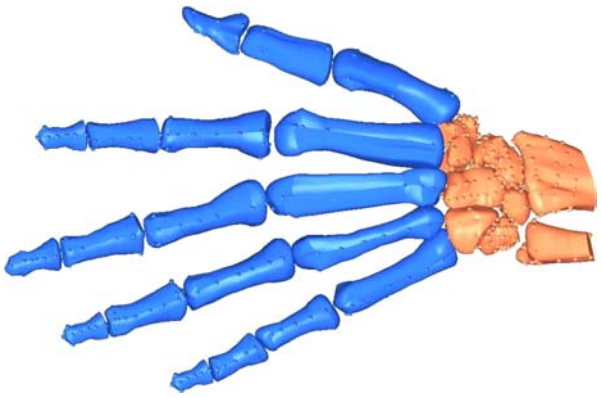

Figure 4. Surface reconstruction based on STL meshing: wrist and fingers.

The final mesh of the hand includes (Figure 6):

- Eight bones of the wrist (carpsal): the scaphoid, lunate, triquetral pisiform, trapezium, trapezoid, capitate and hamate.
- Five metacarpsal.
- 14 phalanges: distal phalanges, middle phalanges and proximal phalanges.

3.2 Description of the impact problem

The numerical example presented in this section shows how a hand gets into contact with an object. It is a very useful first step to simulations of hand and hand-held tool interactions to improve design.

Our work consists in setting up a finite model of a hand as biofidelic as possible. The creation of this kind of model needs many investigations and leads to extremely complicated FE model, generally CPU time consumer. The hand is composed of different components (cartilage, tendons, ligaments and muscles). The influence of these individual components may be essential to the overall response of the hand. Our model is a first step in the creation of a hand model: no cartilage, no tendons, no ligaments and no muscles are taken into account. Actually, the behaviour of skin and all soft tissues is processed by the HGO model presented in Section 2.2.

The object is considered as linear elastic. Discrepancies exist concerning the elasticity of the cortical bone. Age dependency has been demonstrated, which varies between 10 and 15 GPa (Rho et al. 1997; Wang et al. 2002; Kemper et al. 2005; Buchanan and Ural 2010). Wrist's and finger's bones are considered as linear elastic with typical cortical bones's properties: $E = 10,000\,\text{MPa}$, $\nu = 0.22$ and $\rho = 2150\,\text{kg/m}^3$.

The hand sizes corresponding to $L_1 = 159.23$, $L_2 = 230.12$ and $L_3 = 77.68\,\text{mm}$ are shown in Figure 7, whereas the block ones are shown in Figure 8. The hand mesh is described in Figure 6 with 5794 nodes and 17,700

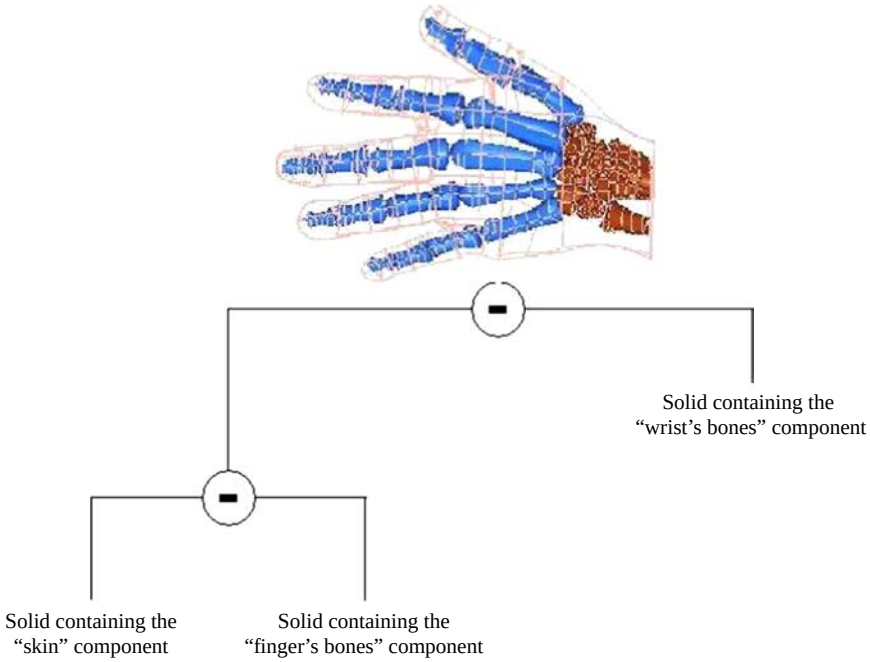

Figure 5. Description of the creation of the mesh.

tetrahedral elements. Besides, the parallelepipedic block has 1040 nodes and 4684 tetrahedral elements.

3.3 Numerical strategy

The treatment of contact conditions leads to variational inequalities. Various algorithms could be employed to solve contact problems. In this paper, we have chosen to use an original approach, the bi-potential method, which has been successfully applied for the modelling of frictional contact problems in static cases. This paper presents the application of this method for dynamic analysis of impact problems with friction between an hyperelastic body and an elastic one (Feng et al. 2006).

We want to model an operator’s hand at work, but its movement control depends on the rigidity of the hand gesture. We assume that the hand manipulates the block using an initial speed equal to $v_0 = 2\,\mathrm{m/s}$ in the x-direction (Figure 8). The transient dynamic calculation is managed by an explicit scheme shown in Section 2.2.2 to cut down computational cost. This choice is justified by the highly nonlinear feature of the case, as it deals with the dynamic contact and impact in 3D anisotropic hyperelasticity. The explicit resolution of contact problem is much more efficient than the implicit one because it is well adapted to speed and acceleration discontinuities when a sudden contact status change occurs. Accordingly, the decision of using an explicit contact FE model appears rational.

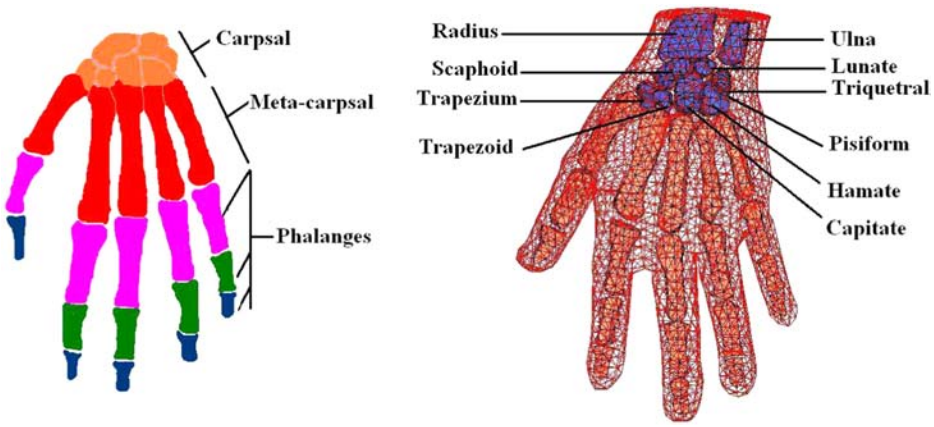

Figure 6. Final mesh of the hand.

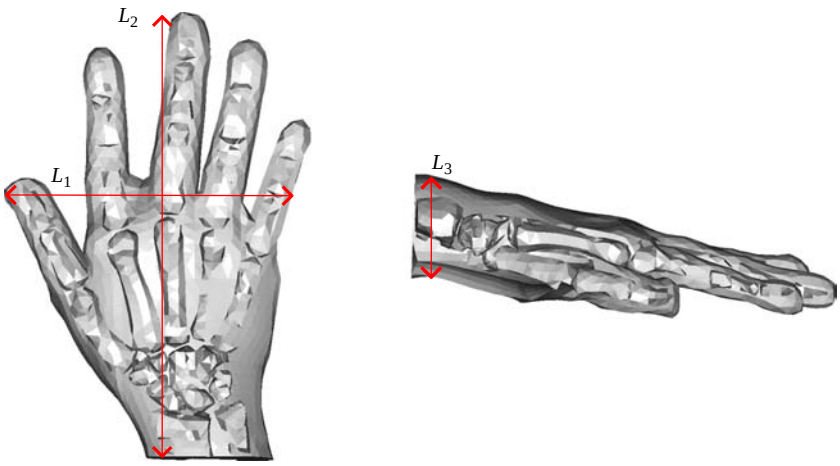

Figure 7. Hand sizes.

It has been shown that non-linearity can cause divergence using an implicit FE code (Horii et al. 1993). An explicit analysis requires the identification of a critical time step to ensure the stability of the temporal scheme (Newmark 1959). This critical time step is related to the characteristic element size and material properties. A critical value can be defined as the time required such that the pressure wave travels through only one elastic element:

$$\Delta t = \sqrt{\frac{\rho}{E}} L_{\min}, \tag{36}$$

$L_{\min}$ is the characteristic dimension of the smallest mesh element, ρ is the density and E is the Young modulus. The magnitude of $L_{\min}$ is 10^{-5}m in the case of this study. A time step has been chosen approximatively equal to 10^{-7}s. The analysis was carried out using the FE code FER.

Figure 9 shows the stress on a cross-sectional plane on the bones as well as on the soft tissue.

3.4 Results

Figure 10 shows the evolution over time of the von Mises stress at different steps of computation: $t = 0.002$, $t = 0.003$, $t = 0.004$ and $t = 0.005$ s. Since stresses begin in the contact areas between the hand and the block, it is possible to track the spread of the contact areas during the time.

4. Discussion and future work

Our main interest and motivation for this research are to develop a simplistic yet sufficiently accurate model that can describe hand motion and its contacts during reach and grasp operations. Many grasping models (Kim et al. 2009; Bae and Armstrong 2011; Carbone and González 2011) have already been developed but none of them use a 3D total deformable hand model, which means there are limitations to these models in terms of modelling deformity during contacts. Contrary to the above models, this research shows precisely the dynamic stress and its

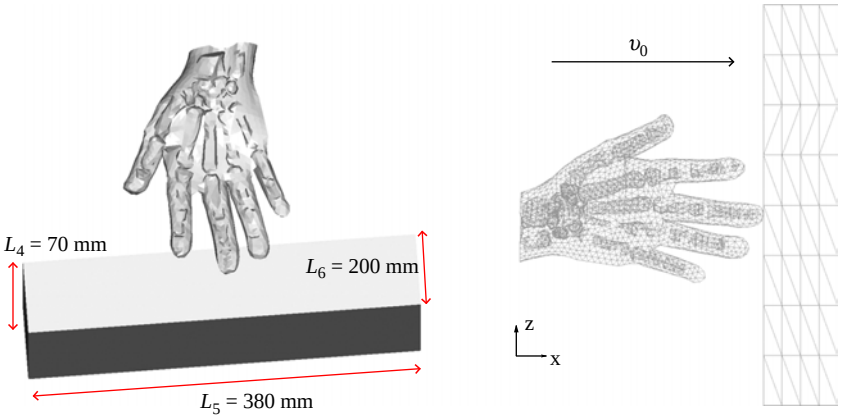

Figure 8. Problem description.

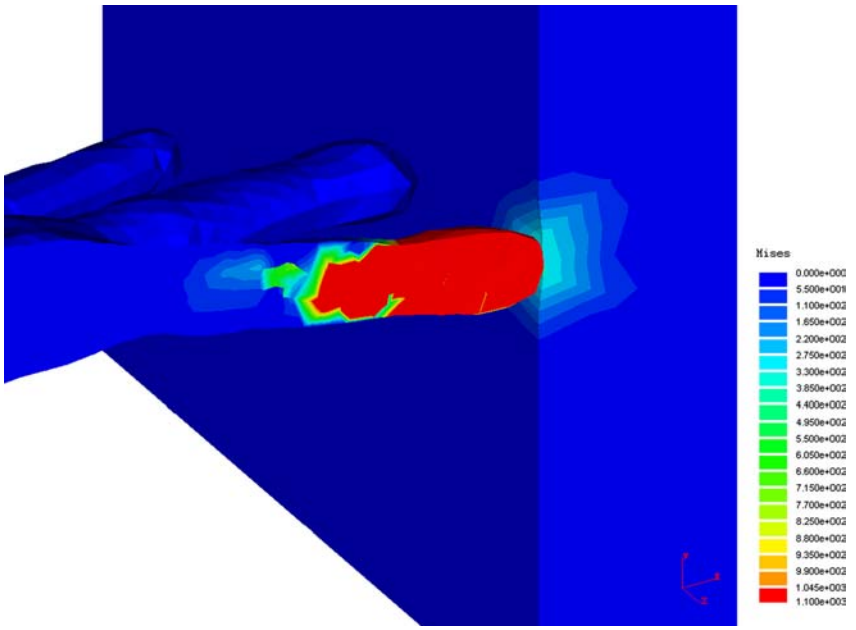

Figure 9. Von Mises stress.

changes for any part of the hand or finger and this represents a step advancement in hand modelling. In this research, the FE method has been chosen to model these phenomena to overcome the above deficiency. This approach has presented a big challenge for two main reasons. From a mechanical point of view, multiple nonlinearities must be taking into account in geometrical, material, frictional contact and impact modelling. From a biomechanical point of view, a much better knowledge of the hand's biomechanical capability as well as limitation must be understood in order to develop a closer representation of a real hand. On that basis, this model, in fact, is only a first step to create a more realistic hand model. The main purpose of this paper is to validate a process of converting a CT scan to a 3D FE model and then performing a simulation on this model considering the nonlinear phenomena such as contact and hyperelasticity. The paper is not focused on the detailed structures of the hand tissues. Authors believe that based on the current modelling techniques and methods, it is very difficult to generate a numerical model that can represent 100% complexity of the hand for a speed critical application if possible. The proposed model is simplistic from the biomechanical point of view, but the model is sufficient from a functional and mechanical point of view and for many applications similar to the case study. The cartilage, tendons, ligaments and muscles do not play an important individual role and can reasonably be lumped or simplified into one model. The next step of our work will be concerned with a detailed biomechanical modelling of the movements of reaching and grasping, linking to different tissues. The idea is to combine soft tissue with appropriate comportment law (Natali et al. 2006; Evans 2009) and an articulated model for the skeleton. Figure 11 shows the first evolution of the model with an example of movement of grasping tool. This model takes into account ligaments modelled as springs, and the use of anisotropic hyperelasticity is the next step. In addition, experimental work has been done for the tendons, especially for patients with arthritis conditions. These experimental data are being analysed and processed to form a model to take account of tendons and the models presented in this paper in another paper.

5. Conclusion

The main purpose of this paper is to present an FE solution of large deformation contact/impact problems with Coulomb friction and anisotropic hyperelastic bodies. This problem includes multiple nonlinearities: geometrical, material, frictional contact and impact. The above numerical results demonstrate that the proposed algorithms for the local analysis of frictional contact and impact problems, and for the global resolution of nonlinear equation related to anisotropic hyperelastic materials, are able to handle bioengineering applications. The anisotropic hyperelastic HGO material modelling soft tissues behaviour and the bi-potential method used to solve the contact problem were implemented in the in-house FE code FER. These implementations are detailed in the paper. To demonstrate the efficiency of FER to deal with the nonlinear topics considered in this paper, a numerical example is presented. This example concerns the

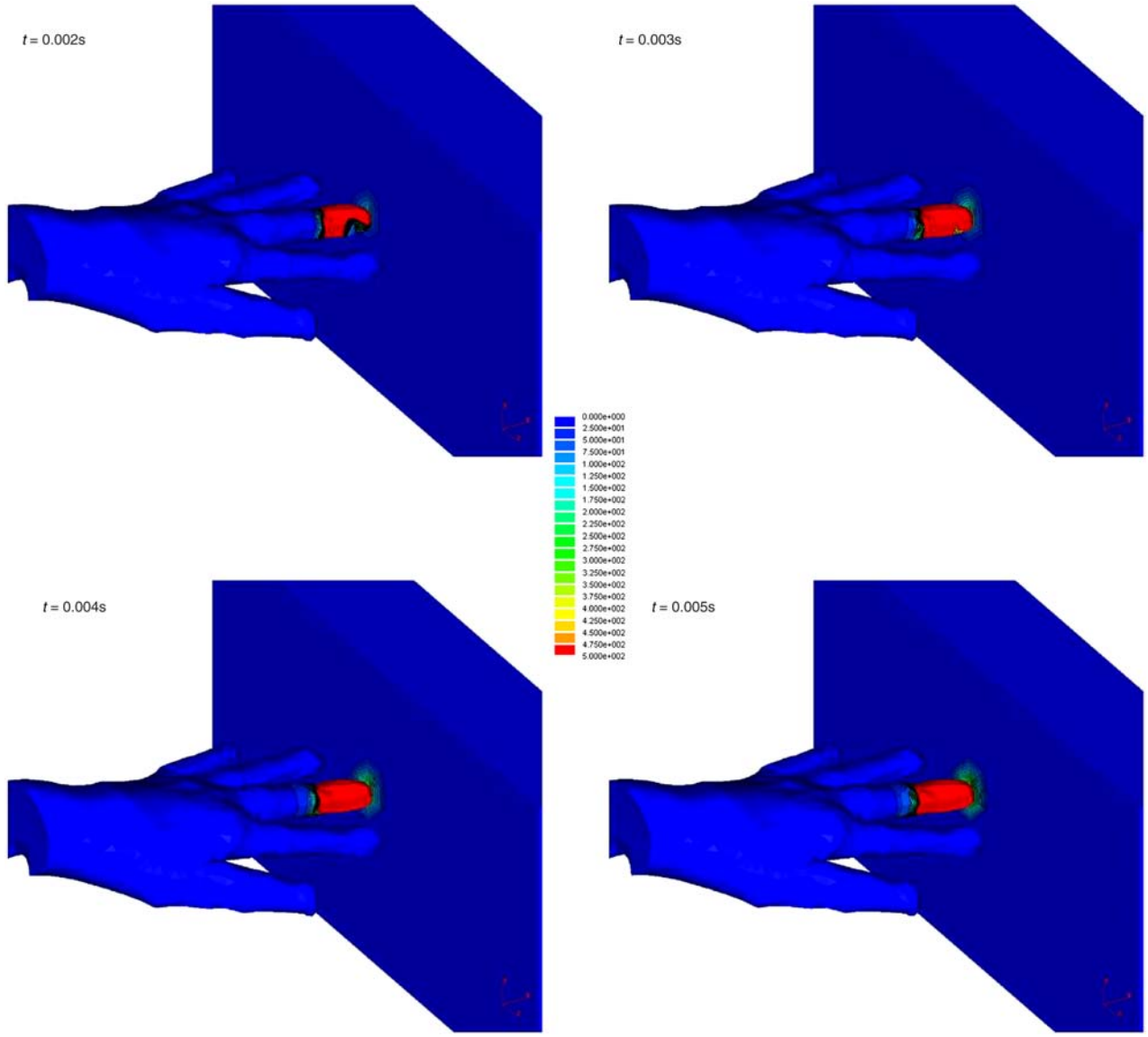

Figure 10. Evolution of the Von Mises stress.

contact/impact of a human hand on a deformable rectangular block. The modelling of the hand includes the bones and the soft tissues' behaviours. Our work paves the way to modelling surgery environment by using the FE simulation. However, including such model in the context of virtual reality (for example to train surgeons to good practise and adequate gestures) is still a challenging task as the computation time does not meet the requirement for the real-time application. Contact detection in a reduced basis (generally used by model reduction techniques to drastically save computation time) is also another open issue.

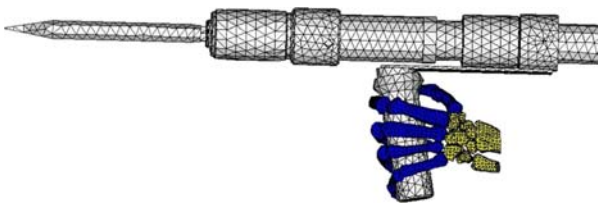

Figure 11. Work in progress: movements of grasping.

References

Alart P, Curnier A. 1991. A mixed formulation for frictional contact problems prone to Newton like solution methods. Comput Meth Appl Mech Eng. 92(3):353–375.

Almeida ES, Spilker RL. 1998. Finite element formulations for hyperelastic transversely isotropic biphasic soft tissues. Comput Methods Appl Mech Eng. 151(3–4):513–538. Containing papers presented at the symposium on Advances in Computational Mechanics.

Bae S, Armstrong TJ. 2011. A finger motion model for reach and grasp. Int J Ind Ergon. 41(1):79–89.

Balzani D, Neff P, Schröder J, Holzapfel GA. 2006. A polyconvex framework for soft biological tissues. Adjustment to experimental data. Int J Solids Struct. 43(20):6052–6070.

Boehler JP. 1987. Introduction to the invariant formulation of anisotropic constitutive equations. Applications of tensor functions in solids mechanics, CISM Course No. 292. Springer Verlag.

Buchanan D, Ural A. 2010. ASME; finite element modeling of the influence of hand position and bone properties on the Colles' fracture load during a fall. J Biomech Eng. 132(8):081007.

Carbone G, González A. 2011. Tarrytown, NY: Pergamon Press, Inc.; A numerical simulation of the grasp operation by LARM Hand IV: a three finger robotic hand. Robot. Comput Integr Manuf. 27:450–459.

Chamoret D, Saillard P, Rassineux A, Bergheau JM. 2004. New smoothing procedures in contact mechanics. J Comput Appl Math. 168(1–2):107–116. Selected papers from the second international conference on advanced computational methods in engineering (ACOMEN 2002).

De Saxcé G, Feng ZQ. 1998. The bipotential method: a constructive approach to design the complete contact law with friction and improved numerical algorithms. Math Comput Model. 28(4–8):225–245.

Evans SL. 2009. On the implementation of a wrinkling, hyperelastic membrane model for skin and other materials. Comput Meth Biomech Biomed Eng. 12(3):319–332.

Feng ZQ, Peyraut F, He QC. 2006. Finite deformations of Ogden's materials under impact loading. Int J Non-Linear Mech. 41(4):575–585.

Feng ZQ, Zei M, Joli P. 2007. An elasto-plastic contact model applied to nanoindentation. Comput Mater Sci. 38(4): 807–813.

Fung YC, Fronek K, Patitucci P. 1979. Pseudoelasticity of arteries and the choice of its mathematical expression. Am J Physiol Heart Circ Physiol. 237(5):H620–H631.

Gasser TC, Ogden RW, Holzapfel GA. 2006. Hyperelastic modelling of arterial layers with distributed collagen fibre orientations. J R Soc Interface. 3(6):15–35.

Guo ZY, Caner F, Peng XQ, Moran B. 2008. On constitutive modelling of porous neo-Hookean composites. J Mech Phys Solids. 56(6):2338–2357.

Holzapfel GA, Gasser TC, Ogden RW. 2000. A new constitutive framework for arterial wall mechanics and a comparative study of material models. J Elasticity. 61(1):1–48.

Horii E, An KN, Linscheid RL. 1993. Excursion of prime wrist tendons. J Hand Surg. 18(1):83–90.

Joli P, Feng ZQ. 2008. Uzawa and Newton algorithms to solve frictional contact problems within the bi-potential framework. Int J Numer Meth Eng. 73:317–330.

Kemper AR, McNally C, Kennedy EA, Manoogian SJ, Rath AL, Ng TP, Stitzel JD, Smith EP, Duma SM, Matsuoka F. 2005. Material properties of human rib cortical bone from dynamic tension coupon testing. Stapp Car Crash J. 49:199–230.

Kim Y, Choi J, Park J. 2009. Physically based grasping and manipulation method using pre-contact grasping quality measure. In: Proceedings of the 16th ACM symposium on virtual reality software and technology. Kyoto, Japan. VRST'09. New York, NY: ACM. p. 253–254.

Misra S, Ramesh KT, Okamura AM. 2010. Modelling of non-linear elastic tissues for surgical simulation. Comput Meth Biomech Biomed Eng. 13(6):811–818.

Natali A, Carniel E, Pavan P, Dario P, Izzo I. 2006. Hyperelastic models for the analysis of soft tissue mechanics: definition of constitutive parameters. In: Biomedical robotics and biomechatronics, 2006. BioRob 2006. The First IEEE/RAS-EMBS international conference on, p. 188–191.

Newmark NM. 1959. A method of computation for structural dynamics. J Eng Mech Division. ASCE. 85(EM3):67–94.

Peng XQ, Guo ZY, Moran B. 2006. ASME; an anisotropic hyperelastic constitutive model with fiber-matrix shear interaction for the human annulus fibrosus. J Appl Mech. 73(5):815–824.

Peyraut F, Chamoret D, Gomes S, Feng ZQ. 2010. Implémentation éléments finis du modèle hyperélastique anisotrope HGO. Eur J Comput Mech. 9:441–464.

Rho JY, Tsui TY, Pharr GM. 1997. Elastic properties of human cortical and trabecular lamellar bone measured by nano-indentation. Biomaterials. 18(20):1325–1330.

Rüter M, Stein E. 2000. Analysis, finite element computation and error estimation in transversely isotropic nearly incompressible finite elasticity. Comput Meth Appl Mech Eng. 190(5–7): 519–541.

Schröder J, Neff P, Balzani D. 2005. A variational approach for materially stable anisotropic hyperelasticity. Int J Solids Struct. 42(15):4352–4371.

Scovazzi G, Love E, Shashkov MJ. 2008. Multi-scale Lagrangian shock hydrodynamics on Q1/P0 finite elements: theoretical framework and two-dimensional computations. Comput Meth Appl Mech Eng. 197(9–12):1056–1079.

Simo JC, Laursen TA. 1992. An augmented Lagrangian treatment of contact problems involving friction. Comput Struct. 42(1):97–116.

Spencer AJM. 1987. Isotropic polynomial invariants and tensor functions. In: Applications of tensor functions in solids mechanics, CISM Course No. 292. Springer Verlag.

Thalmann NM, Thalmann D. 1995. Finite elements in task-level animation. Finite Elem Anal Des. 19(4):227–242.

Wang X, Shen X, Li X, Agrawal CM. 2002. Age-related changes in the collagen network and toughness of bone. Bone. 31(1):1–7.

Weiss JA, Maker BN, Govindjee S. 1996. Finite element implementation of incompressible, transversely isotropic hyperelasticity. Comput Meth Appl Mech Eng. 135(1–2): 107–128.

Zhang JM, Rychlewski J. 1990. Structural tensors for anisotropic solids. Arch Mech. 42:267–277.

Zheng QS, Spencer AJM. 1993. Tensors which characterize anisotropies. Int J Eng Sci. 31(5):679–693.